machines

Article

Analysis of Ball Check Valves with Conical and Spherical Seat Designs from Common-Rail Pumps

Narcis-Daniel Petrea, Razvan-Constantin Iordache and Carmen Bujoreanu *

Mechanical Engineering, Mechatronics and Robotics Department, "Gheorghe Asachi" Technical University of Iasi, 700050 Iasi, Romania
* Correspondence: carmen.bujoreanu@academic.tuiasi.ro

Abstract: Common-rail fuel injection systems are still a good option for equipping new car models. The technology is well known, systems of this type are reliable and can be used on a wide variety of diesel and petrol engines. However, there is still room for improvement. The ball check valve, which is part of the common-rail pump, is designed to open and allow the compressed fluid to be sent to the high-pressure accumulator and close to not allow fuel to return to the compression chamber. The valves' design directly influences the volumetric efficiency of the outlet flow and the robustness against high pressures that lead to low performance and short service life of the fuel injection systems. This paper aims to compare two ball check valves with conical and spherical seat designs. The analysis is based on theoretical calculations and CFD simulations, which will give more confidence in the results. Considering the comparative analysis results, the ball check valve with a spherical seat shows better flow dynamics than the ball check valve with a conical seat. In addition to the improved flow dynamics, the ball check valve with spherical seat seems to have a uniformly distributed fluid pressure inside the valve. In contrast, the conical seat ball check valve has high local fluid pressures, leading to fatigue.

Keywords: common-rail; high-pressure; pump; simulation; flow; valve

check for updates

Citation: Petrea, N.-D.; Iordache, R.-C.; Bujoreanu, C. Analysis of Ball Check Valves with Conical and Spherical Seat Designs from Common-Rail Pumps. *Machines* **2022**, *10*, 959. https://doi.org/10.3390/machines10100959

Academic Editors: Pedro M. B. Torres, Volker Lohweg, Géza Husi, Eduardo André Perondi, Katarzyna Antosz, Oleg Zabolotnyi and Jose Machado

Received: 26 August 2022
Accepted: 18 October 2022
Published: 20 October 2022

1. Introduction

The high-pressure common-rail system has now become the most used injection system globally. It is used on a wide variety of diesel and gasoline engines, which has the advantages of high injection pressure and flexible and adjustable fuel injection, which significantly improve engines' fuel economy, power, and performance [1,2].

Automobile suppliers need to improve their products in the future, and this trend comes from a greater emphasis on environmental protection, where the desire is to optimize efficiency [3].

In the common rail high pressure pump, the hydraulic head is the main sub-assembly that helps to switch from low pressure to high pressure. Two types of purely mechanical valves (with conical seat) are integrated in it, which help in this pressure transformation. There are also several types of valves, with various seat shapes such as elliptical, parabolic, spherical, conical and so on. The design of the seat must ensure a uniform distribution of pressure on large contact surface as possible, thus avoiding the concentration of stresses on narrow areas. In the automotive area, in common rail high pressure pumps, the most used types of valves are those with a conical seat and less other types of valves. Although a new trend is represented by the use of electrically actuated valves [4,5], the introduction of such models in the current system, already in series production, would lead to major design changes. In addition, the introduction of such valves increases the production cost of the entire system. The use of piezoelectric valves is more efficient when integrating them into injectors because the precision of spraying fuel at controlled time intervals leads to optimal engine operation and reduced pollutant emissions.

Since high-pressure pumps have been in series production for a long time, certain failures that lead to total pump damage have been observed in industrial tests. The most affected components are those subjected to high stresses that lead to their premature wear. High pressure valve in the hydraulic head is part of this category.

The ball check valve is a very important component of the common-rail pump, without which it cannot compress the fuel and reach very high pressures [6]. The dynamics or how the valve behaviors when it opens have a significant impact on the common-rail fuel injection system performance [7].

In principle, the desire is to reduce pollutant emissions and reduce fuel consumption for the same or improved performance [8]. Most studies have been performed on fluid flow through the valve and around the sealing element (e.g., ball), in principle for check valves with conical seats. However, incomplete research has been carried out on the check valves with spherical seats [9–12]. The shape of the valve seat is still a critical feature of any valve, but it is not sufficiently studied to bring new improvements, despite the requirements of increased robustness of hydraulic systems [13].

The purpose of this paper is to compare two types of ball check valves, one with a conical seat and one with a spherical seat. An analysis was performed theoretically on conical seat valve and a comparison by computational fluid dynamics simulation (CFD) using ANSYS FLUENT software was realized [14–16]. The final goal is to show which one of these two valves is suitable for a long service life and what technical aspects make the difference. The study investigates differences in the valve performance, such as the valve opening, flow passing through the valve, fluid velocity, fluid flow, and drag of the ball [17–21].

Literature focused on improving conical seat valves because they are easy to produce, inexpensive and can be used on a multitude of applications, but few on spherical seat valves. Therefore, the paper provides a technical comparison between the two types of valves and highlights the advantages of the spherical seat valves. Considering the spherical seat solution, the service life and performance of the basic system is improved because the fluid flow dynamics are smoother, and the mechanical stresses are lower.

2. Hydraulic Head Assembly Components

The hydraulic head is part of the high-pressure pump assembly. With the plunger, inlet and outlet valve, the hydraulic head can compress and deliver fuel at pressures over 2000 bar to the high-pressure accumulator.

The hydraulic head components are exemplified in the part section from Figure 1.

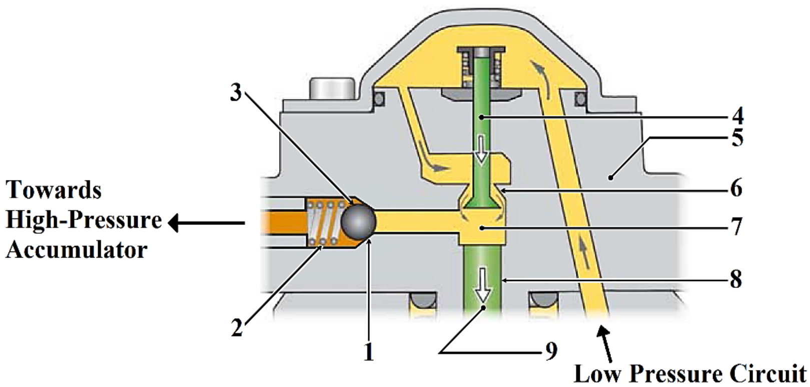

Figure 1. Hydraulic head assembly with valves and plunger [22]. 1—Outlet valve seat; 2—Outlet valve spring; 3—Outlet valve ball; 4—Inlet valve stem; 5—Hydraulic head body; 6—Inlet valve seat; 7—Compression chamber; 8—Plunger bore; 9—Plunger.

The ball check valve should prevent reverse flow in a system [23]. Usually, ball check valves are placed in the discharge pipe, immediately after the pump, where a single directional flow is desired. The basic requirements for check valves are: low resistance in the positive flow direction and infinite resistance in the negative flow direction, which means no leakage [24].

Figure 2a shows a ball check valve with a conical seat and, in Figure 2b, one with a spherical seat.

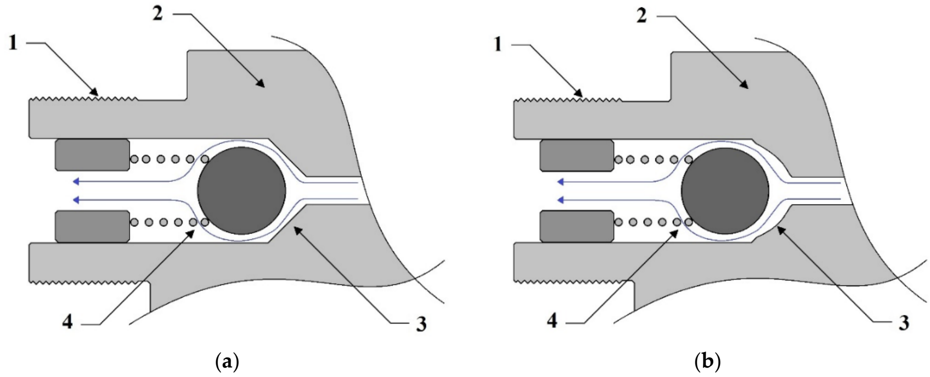

Figure 2. (**a**) Ball check valve with conical seat; 1—Connection to the high-pressure accumulator; 2—Hydraulic head body; 3—Conical seat; 4—Spring; (**b**) Ball check valve with spherical seat; 1—Connection to the high-pressure accumulator; 2—Hydraulic head body; 3—Spherical seat; 4—Spring.

The ball check valve design with conical seat is widely used, and the advantage of this design is that the ball self-centers as it moves toward the seat because it is tangent to the cone. The machining tolerances for this design are not very restrictive [25].

Instead, the design of the spherical seat valve withstands much higher sealing forces. The machining tolerances for this design are quite tight because the ball must reach precisely the center of the spherical seat. This type of design requires a round cone and a good concentricity between the cone and the fluid passage hole.

3. Theoretical Analysis

The ball check valve's performance can be calculated by knowing a predefined set of information about the common-rail system to which it belongs. The rotational speed of the high-pressure pump is not always the same as rotation speed of the engine, existing different transmission ratios. In our case, the common-rail injection system consists of a high-pressure pump to which its driveshaft is mechanically connected to the engine's crankshaft at a transmission ratio of 1:1, which means that the engine speed is the same as the high-pressure pump's speed [26].

The pressures in the compression chamber (p_{up}) and in the high-pressure accumulator (p_{dn}) are necessary for the theoretical calculations, and their values, which can be observed in Table 1, were defined based on experimental tests [26,27].

Table 1. Typical working pressures depending on the speed of the pump.

Common-Rail Pump Speed [rpm]	High-Pressure Accumulator Pressure (p_{dn}) [bar]	Compression Chamber Pressure (p_{up}) [bar]
100	100	120
800	300	330
2000	1600	1680
4000	2000	2100
5000	2000	2100

As observation, even if the engine does not start at 100 rpm, it was considered in our analysis as reference point for the valve functioning (a small valve opening is realized). Maximum common rail pump speed is considered to be 5000 rpm due to manufacturer safety specifications.

Fluid temperature is important in calculations because the fluid changes its viscosity and density depending on its value. In a normal operation of the common-rail system, the fuel inlet temperature at the high-pressure pump can vary between 25 °C and 75 °C, and for the analysis, an average temperature of 50 °C has been chosen [28,29].

In Table 2 it can be observed the kinematic viscosity (ν) with dynamic viscosity (μ) and density (ρ) values at the temperature of 50 °C.

Table 2. Diesel properties at temperature of 50 °C.

Fluid Temperature (°C)	Kinematic Viscosity (ν) [cSt]	Dynamic Viscosity (μ) [mPa·s]	Density (ρ) [g/cm^3]
50	1.96	1.45	0.82

3.1. Simplified Ball Check Valve Modelling

To study a ball check valve's behavior from a theoretical point of view, a simple sketch with the representation of the dimensions of interest is required. Figure 3 illustrates a ball check valve section with essential dimensional elements required for theoretical calculations. The below elements dimensions are from a real measured piece, with D_S = 3.5 mm, θ = 30° and D_b = 5 mm.

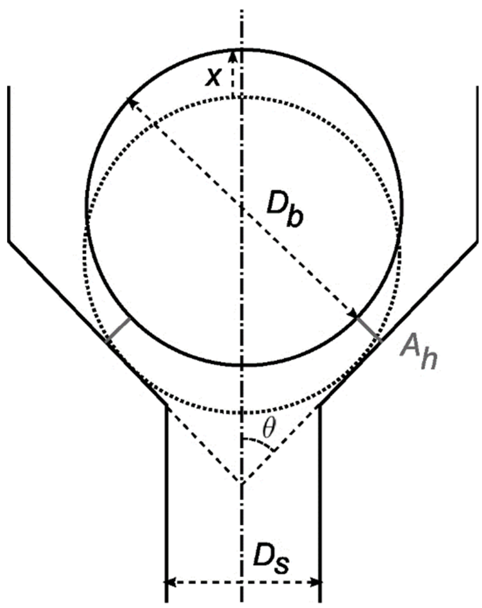

Figure 3. Geometry of the ball check valve [30]. D_S—diameter of the flow section from the compression chamber; D_b—ball diameter; A_h—fluid passage area between the ball and the seat depending on x; x—height of the valve opening (lift); θ—seat angle relative to the axis of symmetry.

The maximum fluid passage area between the ball and the seat can be determined using the following relation:

$$A_{hmax} = \frac{\pi}{4} \cdot D_S^2 \left[mm^2 \right] \quad (1)$$

If the maximum fluid passage area between the ball and the seat is known, in a simplified algebraic model [31], the maximum theoretical valve opening height (x) can be determined using the equation:

$$A_h = \pi \cdot x \cdot \sin\theta \cdot \cos\theta \cdot (x \cdot \sin\theta + D_b) \quad (2)$$

To have a better overview of the valve's performance, it is necessary to observe how it behaves in different operating conditions. This can be carried out after the maximum valve opening height has been determined.

In a simplifying assumption, the high-pressure pump assembly is studied individually, without being mounted on the engine, as it was analyzed in industrial tests [32]. In this hypothesis, increasing the rotation of the pump shaft leads to an increase in the pressure generated by the movement of the piston in the compression chamber and further to an increase in the lifting distance of the ball. Considering these and since the displaced volume of the fluid during the stroke of the piston is constant, we can support the dependence between the rotation of the shaft and the opening of the valve by the following relation:

$$x = \frac{RPM}{RPM_{max}} \cdot x_{max} \ [mm] \quad (3)$$

where:

- RPM—common-rail pump shaft speed;
- RPM_{max}—maximum speed of the common-rail pump shaft;
- x_{max}—maximum valve opening height (lift).

In addition, knowing that the valve opening height varies during operation depending on the pump speed, the flow through the valve can be determined using the following equation:

$$Q_p = d_c \cdot A_h \cdot \sqrt{\frac{2 \cdot \Delta p}{\rho}} \left[\frac{mm^3}{s}\right] \quad (4)$$

where:

- d_c—discharge coefficient;
- Δp—difference between upstream and downstream pressure;
- ρ—fluid density.

The discharge coefficient is considered as the ratio between theoretical and actual flow. It is usually a parameter given by experiments and is used for valve capacity evaluation. It depends on the geometrical properties of the orifice and Reynolds number, and manufacturer data sheets often provide its value [33]. The discharge coefficients of the ball check valve can be considered in a proportional relation to the Reynolds number square root [31]. Their values usually are from 0.6 to 0.8 [34]. Discharge coefficient used for calculations is $d_c = 0.7$.

As well, the difference between upstream and downstream pressure:

$$\Delta p = p_{up} - p_{dn} \ [bar] \quad (5)$$

where:

- p_{up}—upstream pressure (before valve);
- p_{dn}—downstream pressure (after valve);

It is important to know whether the flow passing over a sphere is laminar or turbulent in a hydraulic system [35,36]. Here the Reynolds number is significant and can be determined with the following equation:

$$R_e = \frac{u_h \cdot D_h}{\nu} \quad (6)$$

where: ν is the kinematic viscosity; u_h is the mean flow speed; D_h represents the hydraulic diameter of the ball.

The fluid speed through the fluid passage area provides indications regarding the temperature of the fluid in that area, and a high temperature changes the properties of the material, leading to malfunction of the valve or other system components and even shortening of life due to wear.

The fluid speed through the fluid passage area is determined with the following equation:

$$u_h = \frac{Q_p}{A_h}\ [m/s] \tag{7}$$

Hydraulic diameter means the "characteristic length" and is used to calculate the Reynolds number to determine the flow nature (turbulent or laminar). The hydraulic diameter depends on the lift of the valve and the angle of the seat, and the relationship is as follows:

$$D_h = \sqrt{\frac{4 \cdot A_h}{\pi}}[mm] \tag{8}$$

After determining the flow rates of the fluid through the flow sections, we can also determine the resistance of the fluid when passing over a sphere at different operating regimes of the high-pressure pump where the fluid velocity and flow rate can vary.

The drag force is proportional to three physical quantities: the density ρ of the medium through which the sphere moves, the projected area P_A of the sphere and the speed u_h of the fluid [37]:

$$R = \frac{C_d \cdot \rho \cdot u_h^2 \cdot P_A}{2}\ [N] \tag{9}$$

The projected area of the sphere:

$$P_A = \pi \cdot \frac{D_b^2}{4}\ \left[mm^2\right] \tag{10}$$

In practical applications, the drag coefficient is usually calculated with empirical relations considering experimental data. In a certain range for Reynolds number ($0.2 - 3 \times 10^5$), an approximation formula to determine the drag coefficient C_d of the fluid passing on a sphere is [38,39]:

$$C_d = \frac{24}{R_e} + \frac{6}{1 + \sqrt{R_e}} + 0.4 \tag{11}$$

3.2. Theoretical Results

The obtained theoretical results offer a first perspective on the performance of the ball check valve. Table 3 provides the result of the maximum area through which the fluid can pass from the compression chamber to the valve, also the maximum valve opening height for a ball with a diameter of 5 mm.

Table 3. Maximum theoretical opening height (x) of the valve ball.

Maximum Fluid Passage Area A_{hmax} [mm^2]	Ball Diameter D_b [mm]	Maximum Valve Opening Height [mm]
9.621	5	1.256

Compared to other injection systems, common-rail has the advantage that it can adjust the injection pressure regardless of engine speed [40]. A further advantage of the common rail system is the constant fuel pressure during the injection period [41].

The results depending on engine regime can be seen in Table 4.

Table 4. Height of the valve opening (x) according to the pump speed and the pressure supplied.

Common-Rail Pump Speed [rpm]	High-Pressure Accumulator Pressure (p_{dn}) [bar]	Valve Opening Height (x) [mm]
100	100	0.025
800	300	0.201
2000	1600	0.503
4000	2000	1.005
5000	2000	1.257

Figure 4 shows the pressure in the high-pressure accumulator and the valve opening height, both depending on the high-pressure pump's speed.

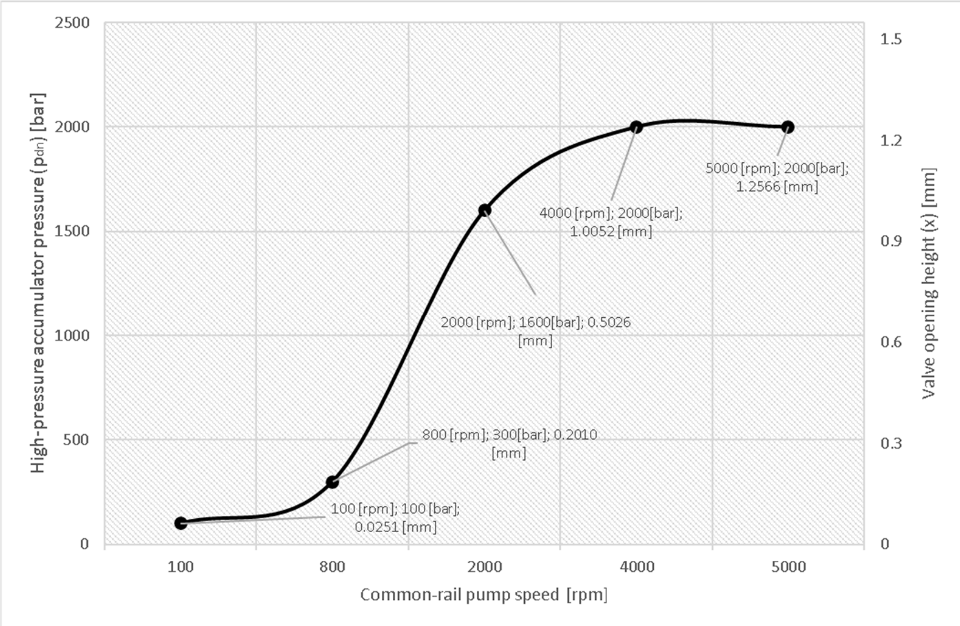

Figure 4. Valve opening according to the pump speed and the pressure supplied.

In this representation, the pressure from the compression chamber (p_{up}) is also important because it influences the valve opening height.

For example, at a pressure request from the injection system of 1600 bar and together with a speed of 2000 rpm of the pump, the valve will open at a pressure in the compression chamber of the pump of 1680 bar, and the opening height of the valve will be of 0.503 mm.

Depending on the high-pressure pump's speed and the pressure in the injection system, the valve opening height is directly influenced. Knowing the valve opening height, the valve opening area and the flow and velocity of the fluid passing through that area were calculated.

The results are listed in Table 5.

Table 5. Opening area, flow and velocity of the fluid through the valve −50 °C.

Valve Opening Height (x) [mm]	Valve Opening Area (A_h) [mm^2]	Flow (Q_p) [l/s]	Fluid Speed through A_h (u_h) [m/s]
0.025	0.171	0.008	48.953
0.201	1.395	0.084	59.955
0.503	3.591	0.351	97.906
1.005	7.525	0.824	109.462
1.257	9.621	1.053	109.462

The graphical representation of the values in Table 5 can be seen in Figure 5, where the valve opening area and the velocity of the fluid passing through that area are illustrated, depending on the valve opening height.

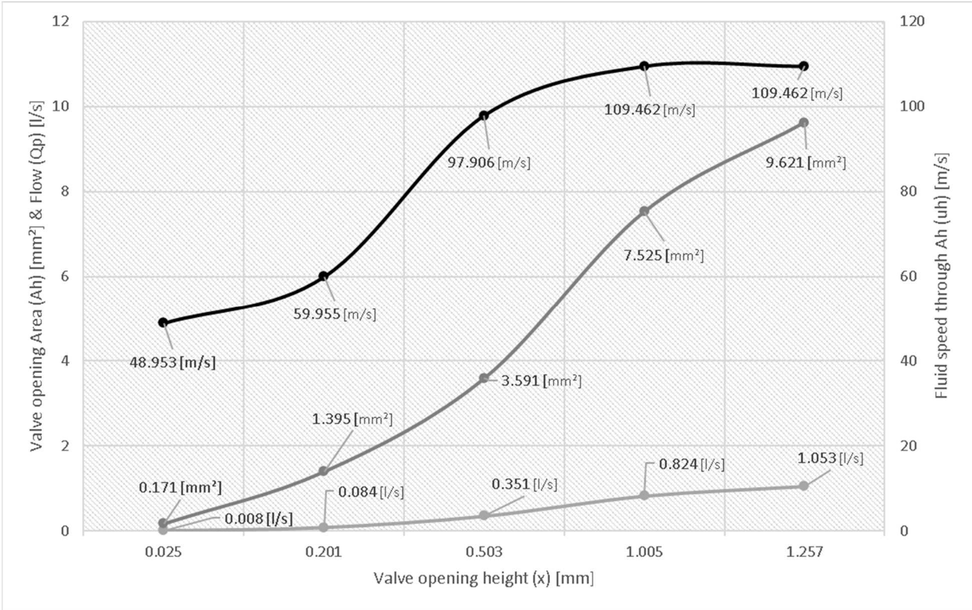

Figure 5. Opening area, flow and velocity of the fluid through the valve −50 °C.

For example, at a valve opening height of 0.503 mm, the injection system's pressure is approximately 1600 bar, and the fluid passage area is 3.591 mm^2, respectively, a flow rate of 0.351 L/s and a speed of the fluid of 97.906 m/s.

The drag force for a sphere in a fluid in which the system pressures are very high is a necessity that must be known in the development phase.

Given that the common-rail fuel injection system works at high pressures and calculating the Reynolds number, the values regardless of engine speed are over 10,000 [42].

Table 6 presents the calculated drag forces and Reynolds number over a sphere.

Table 6. Drag of the ball 50 °C.

Ball Diameter (D_b) [mm]	Valve Opening Area (A_h) [mm^2]	Fluid Speed Through A_h (u_h) [m/s]	Drag Coefficient (C_d)	Drag (R) [N]	Reynolds Number (R_e)
5	0.171	48.953	0.457	8.796	11,650
	1.395	59.955	0.430	11.567	40,770
	3.591	97.906	0.419	32.214	106,800
	7.525	109.462	0.400	38.501	172,900
	9.621	109.462	0.400	38.499	195,500

The speed of the fluid passing through the area between the ball and the seat, the projected area of the sphere, the density of the fluid and the calculated coefficient of resistance give the values of the theoretical drag force on the sphere at all engine operating regimes.

In Figure 6, we can observe the speed of the fluid passing through the ball and seat, the drag coefficient and the drag force. All this depends on the opening of the valve, which is also influenced by the engine speed and the system's pressure.

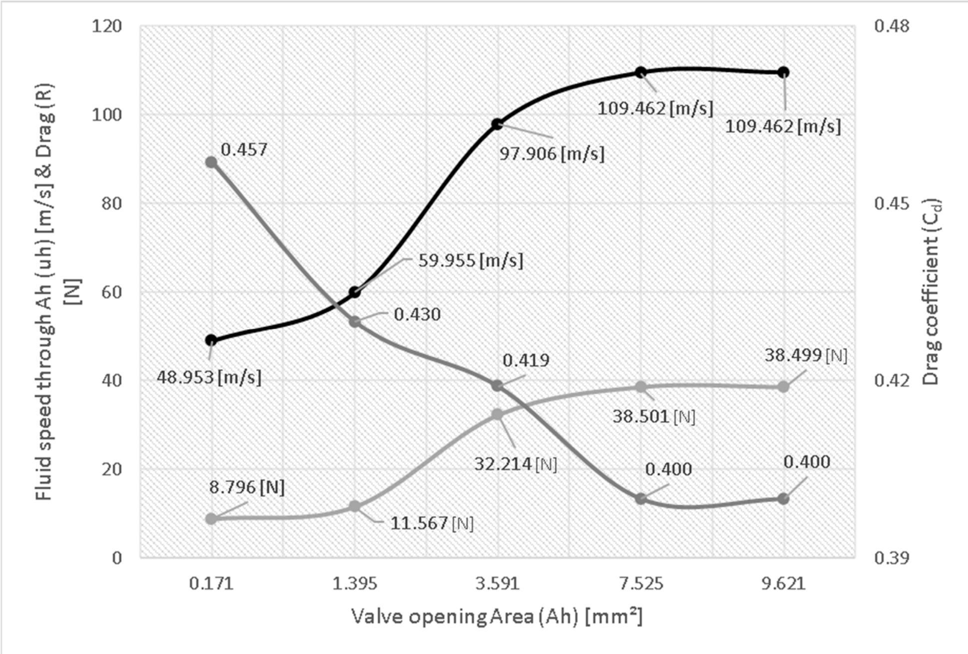

Figure 6. Drag of the ball −50 °C.

For example, at a valve opening of 0.201 mm, we have a fluid velocity of 59.955 m/s, a drag coefficient of 0.430 and a drag force of 11.567 N, respectively.

4. CFD Analysis

Computational fluid dynamics has become a necessary tool for most applications in science and engineering. The numerical methods used in CFDs can be classified according to the mesh used to discretize a computational domain as structured grid methods, unstructured grid methods, and Cartesian grid methods [9].

The purpose of CFD analysis is to see the differences between the design of the conical and spherical seat valve in terms of pressure, speed and fluid flow lines through the valve, and in the end, it is giving information about which valve design has better performance.

In our analysis, due to slight variations given by different gap sizes between the sphere and the seating profile, the meshing details are extracted from the Fluent solver log the partition method used is METIS with stored partition count 14. There are 35,373 triangular cells, faces count is 54,057 and nodes number is 18,685.

4.1. Pressure CFD Analysis

The pressure CFD simulation is intended to observe how the pressure is distributed inside the valve, to discover the geometry issues that can reduce the valve's performance and if there are risks of concentrated stress areas in which the valve material may break.

Figures 7 and 8 show the pressure distribution inside of two different valve designs, one with conical seat and one with the spherical seat having same parameters, such as the opening height of x = 0.201 mm, pressure in upstream p_{up} = 330 bar and downstream p_{dn} = 300 bar. The pressure is uniformly distributed inside the valve at this running regime, and no concerns can be observed.

The simulation from Figures 9 and 10 show the pressure distribution inside the valves by having the opening height of x = 1.005 mm, pressure in upstream p_{up} = 2100 bar and downstream p_{dn} = 2000 bar. The pressure is much or less uniformly distributed, and what we can observe is that the pressure in the downstream pipe is forming a low-pressure zone for both valve designs.

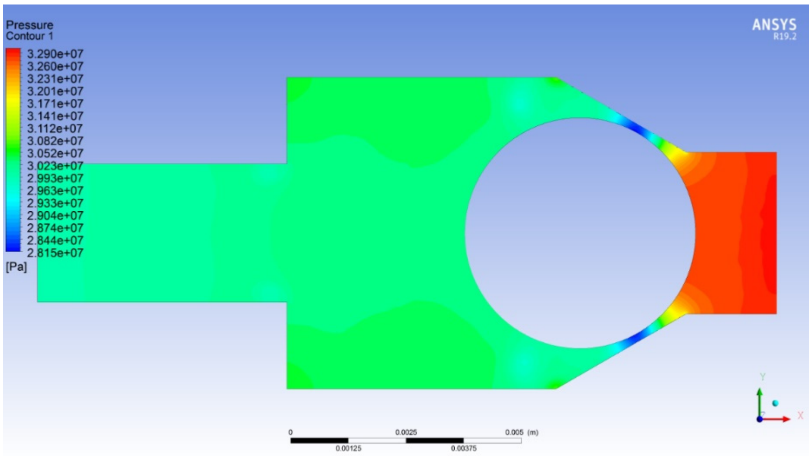

Figure 7. Pressure CFD: Conical seat valve x = 0.201 [mm], p_{dn} = 300 [bar] and p_{up} = 330 [bar].

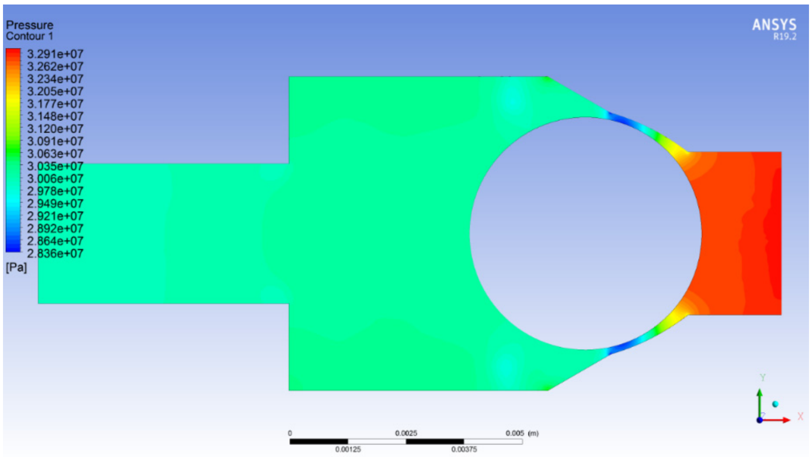

Figure 8. Pressure CFD: Spherical seat valve x = 0.201 [mm], p_{dn} = 300 [bar] and p_{up} = 330 [bar].

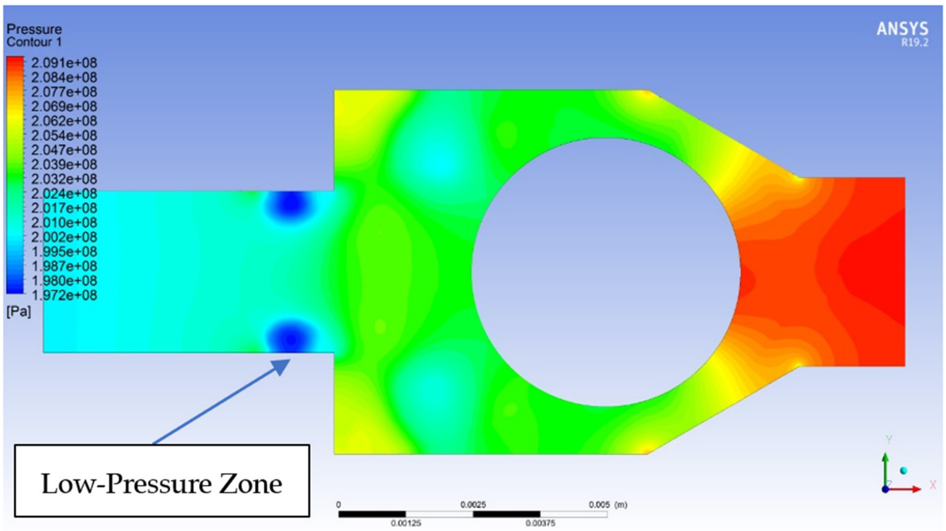

Figure 9. Pressure CFD: Conical Seat Valve − x = 1.005 [mm], p_{dn} = 2000 [bar] and p_{up} = 2100 [bar].

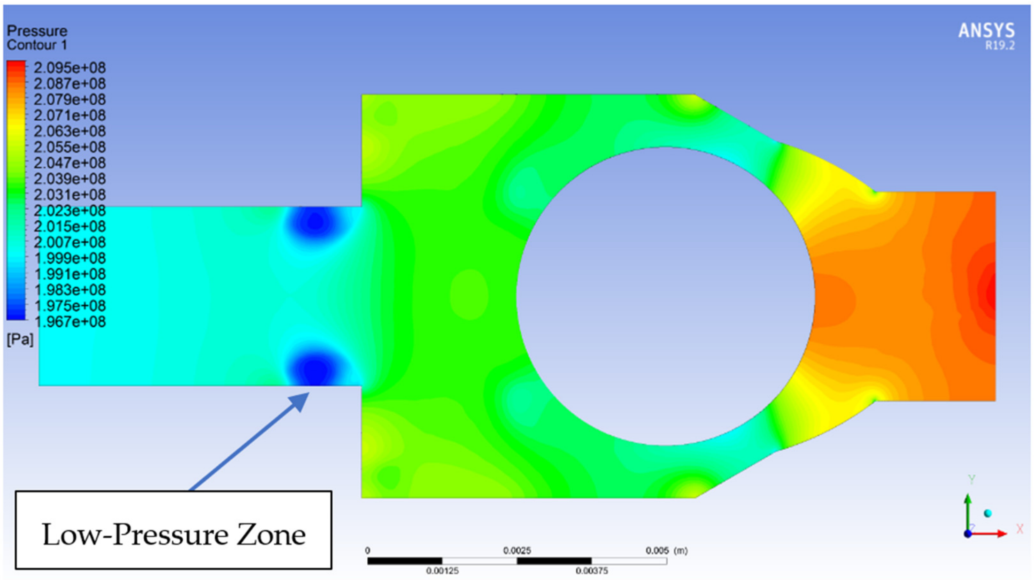

Figure 10. Pressure CFD: Spherical Seat Valve − x = 1.005 [mm], p_{dn} = 2000 [bar] and p_{up} = 2100 [bar].

A low-pressure zone appears in principle due to the design of the valves and together with a high-pressure fluid. The low-pressure zone surrounded by a high-pressure fluid can damage the valve's material by forming bubbles that can implode, and this phenomenon is called cavitation erosion [43].

Figures 11 and 12 are representing two different valves design with the pressure distribution by having the opening height x = 1.257 mm, pressure in upstream p_{up} = 2100 bar and downstream p_{dn} = 2000 bar. It can be seen that the pressure is no longer evenly distributed, and the differences between these two valve models are obvious. Apart from the low-pressure area, which is much smaller for the design of the spherical seat valve, the design of the conical seat valve has a larger area of low pressure compared to the simulation in Figure 9. The simulation also shows for the conical seat valve design a high-pressure area that can affect the valve's integrity, leading to fatigue and cracks in the material [44].

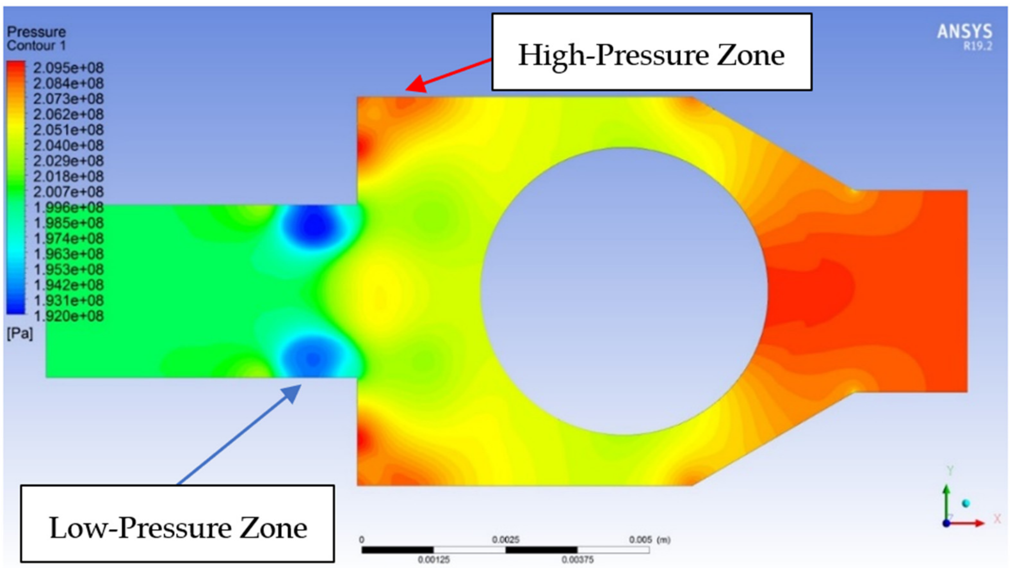

Figure 11. Pressure CFD: Conical Seat Valve − x = 1.257 [mm], p_{dn} = 2000 [bar] and p_{up} = 2100 [bar].

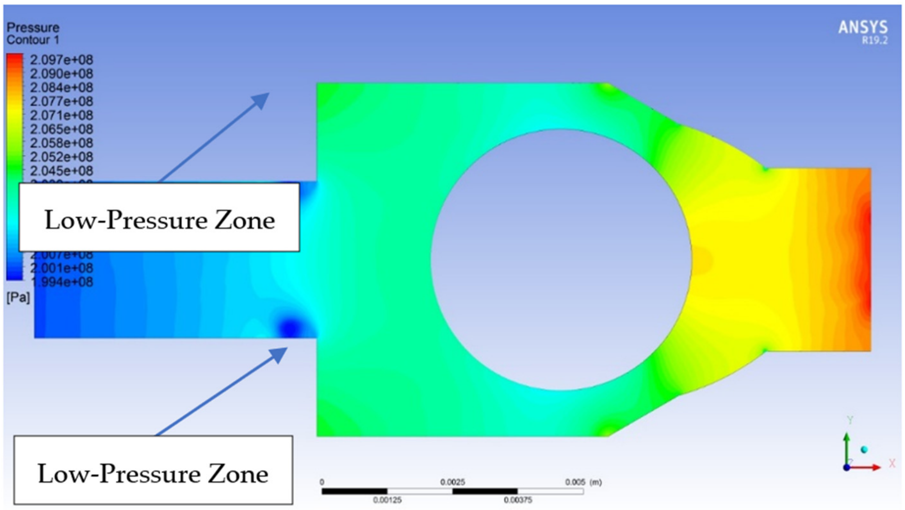

Figure 12. Pressure CFD: Spherical Seat Valve − x = 1.257 [mm], p_{dn} = 2000 [bar] and p_{up} = 2100 [bar].

4.2. Velocity CFD Analysis

Fluid velocity and flow lines were analyzed in order to observe critical areas in the design where fluid flow is affected and lead to reduced valve performance.

Figures 13 and 14 shows the velocity and flow lines going through the two different valve designs, one with conical seat and one with the spherical seat having same parameters, such as the opening height of x = 0.201 mm, pressure in upstream p_{up} = 330 bar and downstream p_{dn} = 300 bar. The speed of the fluid passing through the opening area between the ball and the seat is slightly higher for the conical seat design, and in terms of flow lines, nothing is particularly concerning.

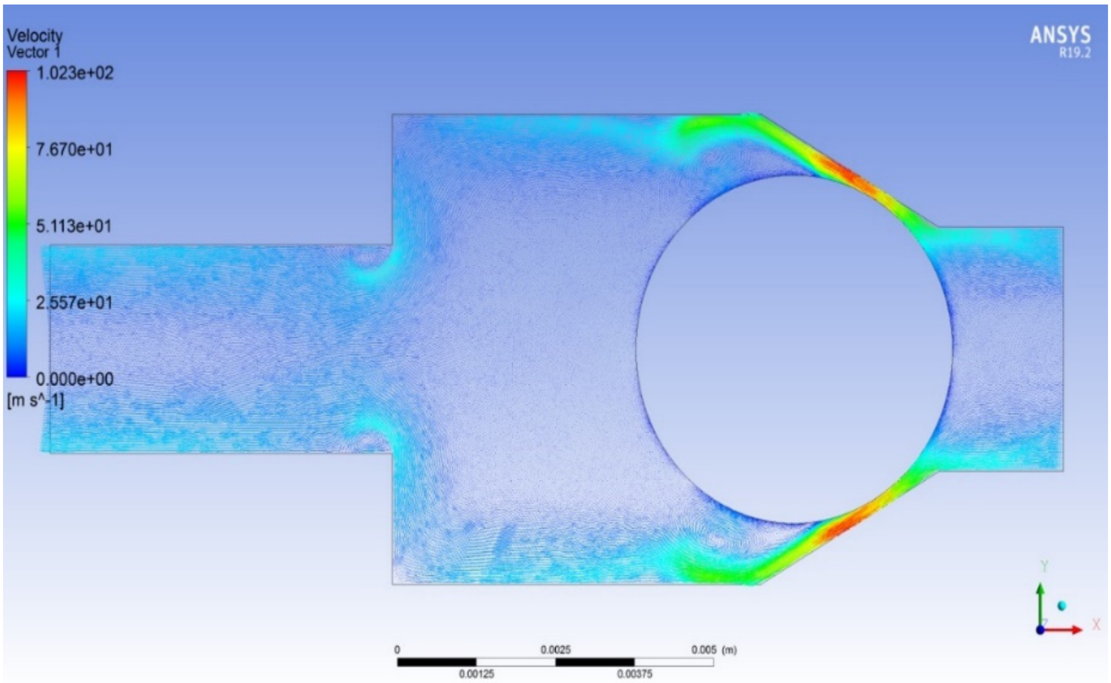

Figure 13. Velocity CFD: Conical Seat Valve: x = 0.201 [mm], p_{dn} = 300 [bar] and p_{up} = 330 [bar].

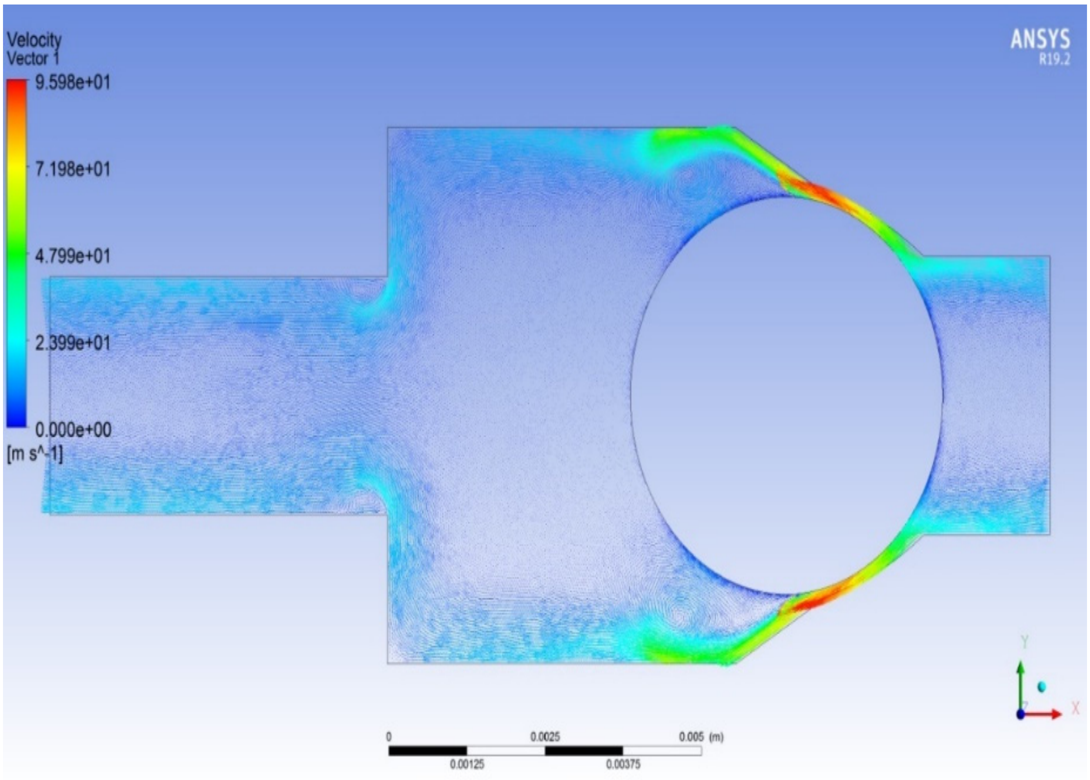

Figure 14. Velocity CFD: Spherical Seat Valve: x = 0.201 [mm], p_{dn} = 300 [bar] and p_{up} = 330 [bar].

Simulation of speed and flow lines shown in Figures 15 and 16 are made with the following parameters, such as the opening height of x = 1.005 mm, the pressure in the upstream p_{up} = 2100 bar and the downstream p_{dn} = 2000 bar. We can notice a small difference regarding the maximum speed of the fluid for the ball valve in the section between the ball and the seat. In the case of the conical seat valve, the area with a high fluid velocity is also larger and can be observed very close to the extremity of the valve diameter, which can lead to a heating of the fluid due to friction with the valve walls and implicitly to reducing valve performance. We can also see that we have a vortex formation in both designs due to the right angle that blocks the uniform flow of fluid [45].

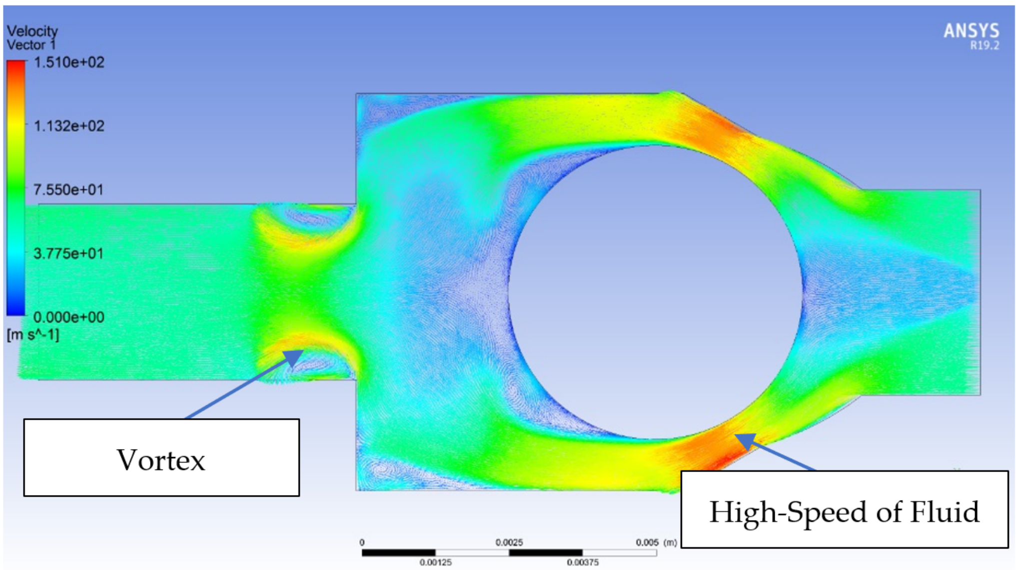

Figure 15. Velocity CFD: Conical Seat Valve: x = 1.005 [mm], p_{dn} = 2000 [bar] and p_{up} = 2100 [bar].

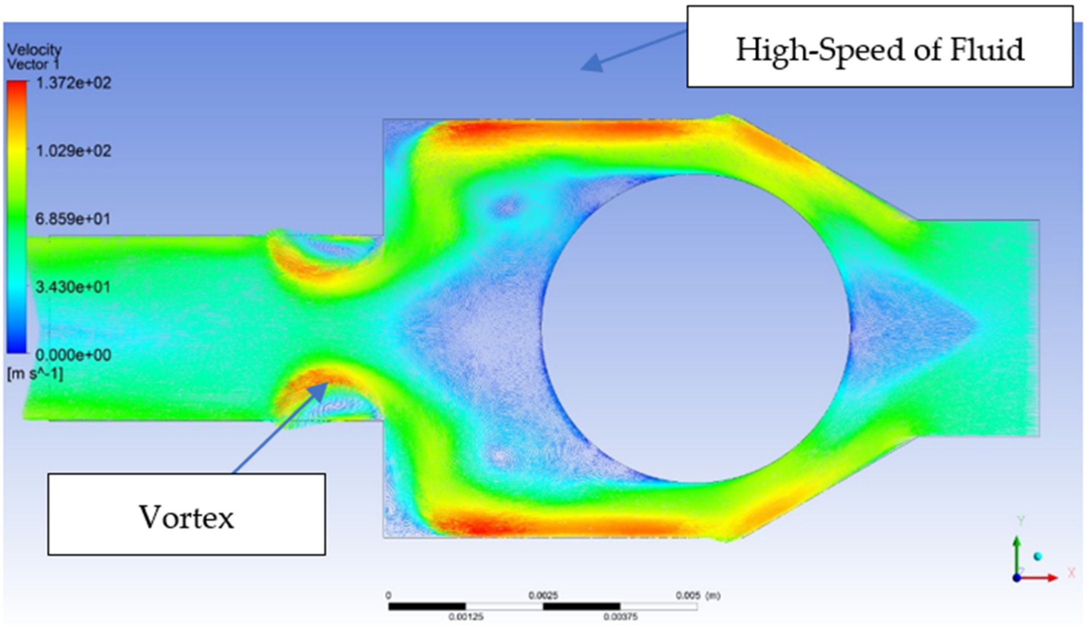

Figure 16. Velocity CFD: Spherical Seat Valve − x = 1.005 [mm], p_{dn} = 2000 [bar] and p_{up} = 2100 [bar].

Figures 17 and 18 are showing two simulations by having the opening height x = 1.257 mm, pressure in upstream p_{up} = 2100 bar and downstream p_{dn} = 2000 bar. First, it can be seen that the maximum fluid velocity for the conical seat design is much higher than the spherical seat design, by 62.5%. The high-speed fluid is present in a vortex, where it is formed due to the shape of the right angle of the valve design. Despite the right-angle shape for both models, the spherical seat design has a much lower fluid velocity, more evenly distributed flow lines through the valve, and a much smaller vortex size than the conical seat design.

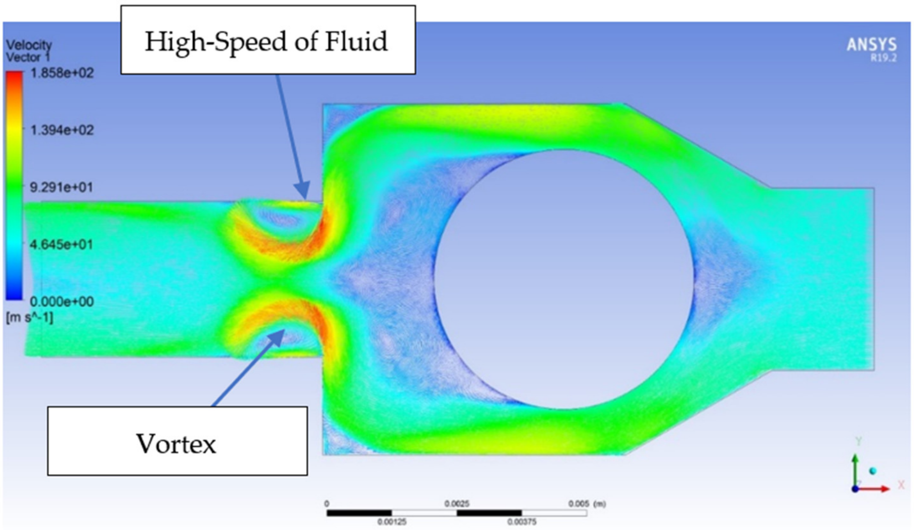

Figure 17. Velocity CFD: Conical Seat Valve: x = 1.257 [mm], p_{dn} = 2000 [bar] and p_{up} = 2100 [bar].

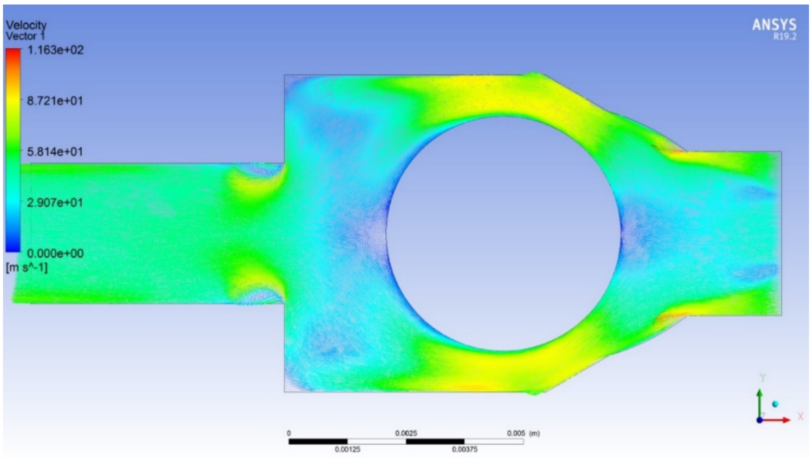

Figure 18. Velocity CFD: Spherical Seat Valve: x = 1.257 [mm], p_{dn} = 2000 [bar] and p_{up} = 2100 [bar].

5. Conclusions

The theoretical analysis has offered values regarding the important parameters of a valve, such as flow, fluid velocity and drag of the ball in a fluid, all depending on the speed of the pump shaft. CFD analysis comes as a complement to theoretical analysis, as it provides a visual representation of pressure, fluid lines, fluid velocity, and it is easy to see where there is a problem with the design, with impact in the performances of valves. The CFD performed has calculated and analyzed steady-state flows at several working points without considering the impact of the spring, so in future work we will focus on this aspect as well. Comparing the two types of valves in CFD simulation, the spherical valve at high pressures in the hydraulic head system shows an improvement in fluid evacuation. This is happening when the fluid reaches the most loaded areas of the valve. These zones are less prone to fluid heating due to friction with the valve wall and formed vortices are much smaller. In addition, the pressure distribution inside the valve is much more uniform, which means that the spherical seat design has another advantage than the conical seat. At a low pressure in the valve, the results of the simulations between the two different valves design are comparable because the differences are insignificant in terms of pressure, fluid lines and fluid velocity.

There is still room for improvement because, as we have seen, the shape of the right angle at the end of the valve causes the formation of a vortex that affects the flow of fluid through the valve and also forms a low-pressure area where cavitation is prone to occur. The work will be expanded in the future with experimental research on the two types of valves assembled in the high-pressure pump, working in real operating conditions. From a practical point of view, the use of a valve with a spherical seat involves the addition of machining operation easy-to-perform with an insignificant production cost. Considering the results obtained, it is recommended to use this type of valve predominantly in the current common rail system.

Author Contributions: Conceptualization, N.-D.P. and C.B.; methodology, N.-D.P. and C.B.; software, N.-D.P. and R.-C.I.; validation, N.-D.P. and C.B.; formal analysis, N.-D.P. and C.B.; investigation, N.-D.P.; resources, N.-D.P. and R.-C.I.; data curation, N.-D.P.; writing—original draft preparation, N.-D.P. and C.B.; writing—review and editing, C.B. and R.-C.I.; visualization, C.B. and R.-C.I.; supervision, C.B.; project administration, C.B.; funding acquisition, C.B. All authors have read and agreed to the published version of the manuscript.

Funding: This research received no external funding.

Institutional Review Board Statement: Not applicable.

Conflicts of Interest: The authors declare no conflict of interest.

References

1. Xu, J.; Hu, H.; Chang, W. Research on Pressure Stability Control of High-pressure Common Rail System Based on Differential Equation Optimization Model. *J. Phys. Conf. Ser.* **2020**, *1549*, 052081. [CrossRef]
2. Osipowicz, T.; Bramek, K.F.; Stoeck, T. Testing of modern common rail fuel injectors. *Combust. Engines* **2015**, *162*, 688–694.
3. Petrea, N.D.; Bujoreanu, C. Importance of fuel injection system for low emissions, combustion noise and low fuel consumption. *IOP Conf. Ser. Mater. Sci. Eng.* **2018**, *444*, 042012. [CrossRef]
4. Ling, M.; He, X.; Wu, M.; Cao, L. Dynamic Design of a Novel High-Speed Piezoelectric Flow Control Valve Based on Compliant Mechanism. *IEEE/ASME Trans. Mechatron.* **2022**, 1–9. [CrossRef]
5. Tamburrano, P.; Amirante, R.; Distaso, E.; Plummer, A.R. Full simulation of a piezoelectric double nozzle flapper pilot valve coupled with a main stage spool valve. *Energy Procedia* **2018**, *148*, 487–494. [CrossRef]
6. Hardy, C.S.; Hudson, C.M.; Harper, M.S.; Ainsworth, D.M. Pressure is nothing without control: Evolution of control valve design. In *Fuel Systems for IC Engines*; Woodhead Publishing: Sawston, UK, 2012; pp. 115–128.
7. Gupta, V.K.; Zhang, Z.; Sun, Z. Modeling and control of a novel pressure regulation mechanism for common rail fuel injection systems. *Appl. Math. Model.* **2011**, *35*, 3473–3483. [CrossRef]
8. Pendzialek, M.; Schneider, J.; Höhe, K.; Zentner, L. Miniaturization of Check Valves. *Mech. Mach. Sci.* **2016**, *45*, 15–26.
9. Yidong, X.; Xiaodong, L.; Hong, L. A Finite Volume Method Based on a WENO Reconstruction for Compressible Flows on Hybrid Grids. In Proceedings of the 52nd Aerospace Sciences Meeting, National Harbor, MD, USA, 13–17 January 2014.
10. Santamaria, A.; Aleker, J. Spring Retaining Sleeve. U.S. Patent US20110089359A1, 21 April 2011.
11. Santamaria, A. Exhaust Valve i.e., Return Valve, for Common-Rail-High Pressure Pump Utilized in Common-Rail-Fuel Injection System, Has Valve Element Comprising Casing and Ball That Is Connected with Casing in Fixed Manner and Guided Indirectly over Casing. Germany Patent DE102010061783A1, 24 May 2012.
12. Masaya, M.; Makoto, T.; Nobuyuki, O. Negative Magnus lift on a rotating sphere at around the critical Reynolds number. *Phys. Fluids* **2012**, *24*, 014102.
13. Elldakli, F.; Soliman, M. Optimum design for new gas lift valve seat. *J. Pet. Sci. Eng.* **2017**, *149*, 456–464. [CrossRef]
14. Lisowski, E.; Filo, G. CFD analysis of the characteristics of a proportional flow control valve with an innovative opening shape. *Energy Convers. Manag.* **2016**, *123*, 15–28. [CrossRef]
15. Hart, J. Comparison of turbulence modeling approaches to the simulation of a dimpled sphere. *Procedia Eng.* **2016**, *147*, 68–73. [CrossRef]
16. Bandari, S.R. Investigation on Flow Control Valve by CFD Simulation. Master's Thesis, Blekinge Institute of Technology, Karlskrona, Sweden, 2017.
17. Perdikaris, P.G.; Kaiktsis, L.; Triantafyllou, G.S. Computational study of flow structure and forces on a cylinder vibrating transversely and in-line to a steady flow: Effects of sub-harmonic excitation. In Proceedings of the Pressure Vessels and Piping Conference, Prague, Czech Republic, 26–30 July 2009; pp. 475–479.
18. Zuhal, L.R.; Dung, D.V.; Sepnov, A.J.; Muhammad, H. Core Spreading Vortex Method for Simulating 3D Flow around Bluff Bodies. *J. Eng. Technol. Sci.* **2014**, *46*, 436–454. [CrossRef]
19. Tofa, M.M.; Maimun, A.; Ahmed, Y.M.; Jamei, S.; Abyn, H. Experimental and Numerical Studies of Vortex Induced Vibration on Cylinder. *J. Teknol.* **2014**, *66*, 169–175.
20. Kurtulus, A.B.; Atmaca, M.; Girgin, I.; Ezgi, C. Forces Acting on and Flow Behind a Sphere. In Proceedings of the ASME-Ati-Uit 2015 Conference on Thermal Energy Systems: Production, Storage, Utilization and the Environment, Napoli, Italy, 17–20 May 2015.
21. Moradian, N.; Ting, D.S.-K.; Cheng, S. The effects of freestream turbulence on the drag coefficient of a sphere. *Exp. Therm. Fluid Sci.* **2009**, *33*, 460–471. [CrossRef]
22. Iordache, R.C.; Petrea, N.D.; Bujoreanu, C. Wear's issues on high-pressure common rail pumps. *IOP Conf. Ser. Mater. Sci. Eng.* **2020**, *724*, 012021. [CrossRef]
23. Kajiwara, S. Effect of the check ball and inlet position on hydraulic L-shaped check ball behavior. *J. Fluids Struct.* **2014**, *48*, 497–506. [CrossRef]
24. Himr, D.; Habán, V.; Hudec, M. Experimental investigation of check valve behaviour during the pump trip. *J. Phys. Conf. Ser.* **2017**, *813*, 012054. [CrossRef]
25. Ball Check Valves. Available online: https://www.precisionballs.com/ball_valve.php (accessed on 19 February 2022).
26. Petrea, N.D.; Bujoreanu, C.; Rîpanu, I.E. Influence of ball-seat contact on the noise emissions from common-rail pump outlet valve opening. *IOP Conf. Ser. Mater. Sci. Eng.* **2018**, *444*, 042012. [CrossRef]
27. Petrea, N.D.; Bujoreanu, C.; Alaci, S. Analysis of the noise emissions of a common-rail pump before and after an endurance test. *IOP Conf. Ser. Mater. Sci. Eng.* **2019**, *591*, 012064. [CrossRef]
28. Pourhoseini, S.H.; Nikzad, R. An experimental study on the effect of inlet diesel fuel temperature on mass flow choking, flame penetration, temperature, radiative characteristics and NOx pollutant emission of an oil burner. *J. Braz. Soc. Mech. Sci. Eng.* **2019**, *41*, 492. [CrossRef]
29. Payr, R.; Salvador, F.J.; Gimeno, J.; Bracho, G. The effect of temperature and pressure on thermodynamic properties of diesel. *Fuel* **2011**, *90*, 1172–1180. [CrossRef]

30. Viel, A. Strong Coupling of Modelica System-Level Models with Detailed CFD Models for Transient Simulation of Hydraulic Components in their Surrounding Environment. In Proceedings of the 8th International Modelica Conference, Dresden, Germany, 20–22 March 2011; pp. 256–265.
31. Mittwollen, N.; Michl, T.; Breit, R. Parametric hydraulic valve model including transitional flow effects. *Math. Model.* **1997**, *11*, 599–604.
32. Iordache, R.C.; Bujoreanu, C.; Petrea, N.D.; Ianus, G. Simulation of high-pressure pump behaviour after running in urban regime. *IOP Conf. Ser. Mater. Sci. Eng.* **2020**, *997*, 012014. [CrossRef]
33. Wei, M.; Cheng, L.; Hongyu, W.; Zhi, Z.; Jianfeng, Z.; Hong, J. Discharge coefficient of pilot poppet valve at low Reynolds number. *Flow Meas. Instrum.* **2022**, *85*, 102141.
34. Hutagalung, S.S. Effect of Release Coefficient of Orifice Plate on Water Fluid Flow Systems. *J. Phys. Conf. Ser.* **2019**, *1230*, 012086. [CrossRef]
35. Doddannavar, R.; Barnard, A. *Practical Hydraulic Systems: Operation and Troubleshooting for Engineers and Technicians*, 1st ed.; Elsevier: Amsterdam, The Netherlands, 2005.
36. Parr, A. *Hydraulics and Pneumatics—A Technician's and Engineer's Guide*, 3rd ed.; Elsevier: Edinburgh, UK, 2011.
37. Al Omari, B. *On the Relation between Radius and Coefficient of Drag*; Waterloo University: Waterloo, ON, Canada, 2020.
38. Dobeš, J.; Kozubková, M. The Influence of Numerical Models on Determining the Drag Coefficient. *EPJ Web Conf.* **2014**, *67*, 02019. [CrossRef]
39. Polezhaev, Y.V.; Chircov, I.V. Drag Coefficient. 2 February 2011. Available online: https://www.thermopedia.com/content/707/ (accessed on 22 August 2022).
40. Jorach, R.; Judge, R.; Annycke, B.; Lamacchia, F. Diesel common rail fuel systems technology for high efficiency ultra low emissions medium duty engines. In *Fuel Systems for IC Engines*; Woodhead Publishing: Sawston, UK, 2012; pp. 141–154.
41. Chen, G.; Chen, C.; Yuan, Y.; Zhu, L. Modelling and Simulation Analysis of High-Pressure Common Rail and Electronic Controlled Injection System for Diesel Engine. *Appl. Math. Nonlinear Sci.* **2020**, *5*, 345–356. [CrossRef]
42. Pantokratoras, A. Flow past a rotating sphere in a non-Newtonian, power-law fluid, up to a Reynolds number of 10,000. *Chem. Eng. Sci.* **2018**, *181*, 311–314. [CrossRef]
43. Liu, D.N.; Yan, Z.J.; Yan, X.L.; Zhu, X.H.; Cheng, D.; Fang, X. Experimental and simulation studies on critical cavitation pressure of oily medium. *IOP Conf. Ser. Mater. Sci. Eng.* **2019**, *504*, 012103. [CrossRef]
44. Haixuan, Y.; Xiao-Lei, X. Fatigue failure of high-pressure oil-pipes of truck diesel engine. *Eng. Fail. Anal.* **2019**, *97*, 145–160.
45. Grinis, L.; Haslavsky, V. Turbulence Modeling Applied to Flow over a Hydraulic Ball Check Valve. *Engineering* **2013**, *5*, 685–691. [CrossRef]